High-order numerical solutions in frequency-independent computational times for scattering applications associated with surfaces with composite roughness

Fernando Reitich‡ and Catalin Turc†

‡ School of Mathematics, University of Minnesota, Minneapolis, MN 55455, USA (reitich@math.umn.edu)

† Applied and Computational Mathematics, California Institute of Technology, Pasadena, CA 91125, USA (turc@acm.caltech.edu)

Abstract. We introduce a new numerical scheme capable of producing, in frequency independent computational times, *high-order* solutions to scattering problems associated with surfaces with composite roughness. The procedure can be interpreted as providing a high-order version of the classical (low-order) two-scale method and, as such, it can produce solutions of significantly higher quality with comparable computational effort. The basic strategy consists of a suitable combination of 1) a *high-order* boundary perturbation treatment [O. Bruno and F. Reitich, *Numerical solution of diffraction problems: A method of variation of boundaries I*, J. Opt. Soc. Am. A **10**, 1993, pp. 1168-1175] that views the highly oscillatory components of the surface as a (possibly large) deformation of the slowly varying portion; and 2) an accurate solution method applicable to *single-scattering* configurations ([O. Bruno, A. Sei and M. Caponi, *High-order high-frequency solutions of rough surface scattering problems*, Radio Science **37**, 2002, 2/1-2/13], [F. Reitich and C. Turc, *High-order solutions of three-dimensional rough-surface scattering problems at high frequencies. I: the scalar case*, Waves Random Complex Media **15**, 2005, 1-16.]) for the sequence of *high-frequency* scattering problems that results from 1), which entails a *fixed*, frequency-independent computational cost. More precisely, the boundary variation procedure in 1) allows for the representation of the fields as a convergent sum of terms which are recursively defined as solutions to scattering problems on the slowly varying portion of the surface, with high frequency incidences that are derived from its highly oscillatory components.

1. Introduction

The difficulties associated with the design of numerical methods capable of simulating accurately the acoustic or electromagnetic scattering from rough surfaces can be largely attributed to 1) the inherent intricacies (e.g. oscillations) of the fields, which become more pronounced at high frequencies (regardless of the geometry), and 2) the specific geometrical details of the scattering surfaces, whose spectra can typically span a range of lengthscales. A wide variety of rigorous numerical solvers (e.g. based on differential, variational and integral equation formulations of the problem) have been developed over the last thirty years which have provided continuously improved capabilities for scattering simulations (see e.g. [1] and the references cited there). Indeed, current state-of-the-art algorithms and hardware can be combined to deliver rather impressive results, in both accuracy and efficiency (see e.g. [2, 4, 5]), for an ever increasing range of configurations. While this trend is certainly expected to continue, this approach is fundamentally limited by the requirement to fully resolve the oscillatory characteristics of the fields and the details of the geometry, a limitation that can prevent its use in a number of important applications. In this paper, we introduce a numerical scheme that, in the context of multi-scale rough surface scattering, can bypass these constraints in the resolution of both field as well as geometrical variations.

The recognition of the aforementioned limitations of rigorous approaches arose, of course, rather early in the development of scattering solvers, and solutions have been sought since. In every case, these have been found in the use of *asymptotic theories* which can provide a means to explicitly incorporate additional information to simplify numerical evaluations. For the problem of high-frequency scattering (cf. 1) above), for instance, these theories may rely on short-wavelength asymptotics; similarly, to deal with differing scales in the scattering geometry (cf. 2)), their separation has been based on perturbation analyses. While the asymptotic nature of these methodologies has been critical in allowing for their successful application in cases wherein rigorous approaches fail, it is also the source of their own restrictions.

Indeed, these theories have classically been derived only to *low order*, e.g. as in the (zero-th order) Kirchhoff approximation (KA) [6, 7] (or its next order correction [8–11]) or the well-known "two-scale" method [7, 12–16] which has limited their applicability. This low-order nature of standard asymptotic approximations was largely due to the mathematical and implementational complications that arise in attempts at increasing their order. As we have recently shown [17, 18] (see also [19]), however, these complexities can be effectively dealt with in the context of high-frequency applications by resorting to integral-equation formulations and *high-order* versions of the classical theory of oscillatory integrals [20]. In this manner, we have demonstrated that high-frequency problems can be resolved with significantly improved accuracy in computational times that are comparable to those required

by classical low-order approaches. In this paper, we extend this approach to allow for the treatment of multiple geometrical scales.

Our approach, initially suggested —though not pursued to any extent— in [21], can be viewed as providing an extension of the two-scale method which can be carried out to arbitrary order, and thus it greatly expands on the applicability of this classical procedure. As its name suggests, the two-scale scheme is based on the separation of the surface into large and small scales (relative to the wavelength of the incident radiation) and on the perspective of viewing the latter as a perturbation of the former. In this manner, the scattering off the underlying long surface scales becomes amenable to a treatment based on high-frequency asymptotics which is, in practice, addressed with KA or its very next order correction. The rough components of the surface, in turn, are accounted for through a perturbative argument that typically retains only the first [22] or, at most, the first two terms in a perturbation series in the amplitude of the small-scale features [7, 23]. While this procedure allows for accurate solutions in limiting cases, the natural restrictions due to the low-order, non-convergent character of the approach significantly confine its domain of applicability.

The method we present here overcomes these limitations by resorting to *high order* expansions in both wavelength, for the resolution of the long scales, and amplitude, for the treatment of the small-scale component of the scattering surfaces. As in the two-scale approach, we make use of a dichotomy in wavenumbers that consists of expressing the multi-scale surface as a (possibly large, in our case) perturbation of a slowly varying surface obtained by truncating the original geometry above a cut-off reference wavenumber [21]. In contrast with the standard low-order versions, however, here we systematically derive a complete perturbation series for the scattered field [24, 25], and we identify each term with the solution of a scattering problem off the slow portion of the surface. These problems derive their incidences from combinations of the high-frequency components of the scattering geometry and they are therefore amenable to a treatment based on (suitable extensions of) a class of high-order high-frequency solvers that we have recently designed [17–19]. Indeed, as we show, these solvers can be extended to allow for the efficient evaluation of high-order *derivatives* of the solutions, as needed in the recursive calculation of successive terms of the perturbation series. With this addition, the overall scheme enables the evaluation of *arbitrarily accurate* solutions in computational times that remain independent of the frequency of radiation, and thus it constitutes a significant improvement over the classical two-scale methods. The class of solvers introduced in [17–19] is based on a phase extraction strategy that is applicable to single-scattering configurations. Generalizations of this procedure to rough surface scattering arrangements that encompass shadowing and multiple scattering effects can be possibly pursued within the framework of localized integration [3] and recently introduced windowed partitions of unity [37].

The developments we present here relate to the multi-scale solver as applied to two-

dimensional scattering problems. For the sake of definiteness we will consider the problem of acoustic scattering from sound soft surfaces (i.e. zero Dirichlet boundary conditions, or, equivalently, HH polarization in electromagnetics), although, as it will be clear, our method can be extended to fully three-dimensional configurations and boundaries of rather general characteristics (see [18, 26]). We begin, in §2, with a review of the basic ideas behind the central components of our approach, namely, those relating to an appropriate high-order perturbation scheme (§2.1) and to a high-order methodology for the evaluation of high-frequency scattering (§2.2). These components are suitably combined in §3 where we detail the overall procedure for the treatment of multi-scale surfaces. The presentation of the algorithm, in §3.1, highlights the need to design an extension of the high-frequency solver to allow for the stable evaluation of high-order derivatives of the field, and an instance of such a scheme is presented in §3.2. Finally, numerical results that exemplify the characteristics of the method are presented in §4, and our conclusions are summarized in §5.

2. Preliminaries

As we have explained above our approach to the simulation of high-frequency scattering events that involve surfaces with composite roughness shall be based on the framework of high-order boundary perturbation methods [24–26] and on the use of some recently derived high-frequency integral-equation schemes [17–19]. For the sake of completeness, here we briefly review (and, in the case of the high-frequency scheme, extend) these procedures with a view towards the description of our approach to multi-scale surfaces in the following sections.

2.1. The method of variation of boundaries [24–26]

The advantages of the use of boundary perturbation methods for calculating scattering returns in problems of electromagnetic and acoustic wave propagation have been recognized now for several decades, since the first order calculation of Rayleigh [27]. Besides the simplicity of their implementations, perturbation approaches generally lead, quite efficiently, to very accurate results within their domain of applicability. Indeed, it was these characteristics that prompted a number of investigations in the last thirty years, mainly in the area of scattering by rough surfaces, and which resulted in a variety of low-order theories [22, 28–34]. The low-order nature of these approaches, of course, restricts their use to the analysis of rather small perturbations of a basic scattering surface, and thus it can severely limit their applicability. Attempts at extending the domain of applicability of these methods by simply raising their order encountered very limited success and led to substantial confusion over the validity of perturbation expansions [35, 36, 40–48].

These limitations were finally overcome in practice in [24–26] (see also [49, 50]) based on theoretical developments that were originally presented in [51]. This latter work clarified the precise domain of validity of perturbative expansions and it led to the incorporation of ideas of analytic continuation [24–26] to significantly extend the capabilities of classical methods based on shape deformations. Specifically, in this context, the solution to the general scattering problem

$$\begin{cases} \Delta u + k^2 u = 0 & \text{in } S^+ = \{\mathbf{x} = (x_1, x_2) : x_2 > S(x_1)\}, \\ u = -\exp\left(i\alpha x_1 - i\beta x_2\right) & \text{on } x_2 = S(x_1), \\ u \text{ satisfies a radiation condition (see e.g. [52]) as } x_2 \to \infty, \end{cases} \tag{1}$$

off a surface

$$x_2 = S(x_1) = S_0(x_1) + F(x_1) \tag{2}$$

is embedded in a family $\{u(\cdot, \delta)\}_{0 \le \delta \le 1}$ that solves (1) with S replaced by

$$S_\delta(x_1) = S_0(x_1) + \delta F(x_1).$$

The original solution then is evaluated from the power series expansion (or its analytic extension [25])

$$u(\mathbf{x}) = u(\mathbf{x}, \delta)|_{\delta=1} = \sum_{n=0}^{\infty} u_n(\mathbf{x}) \delta^n|_{\delta=1} \tag{3}$$

wherein each term can be shown to itself solve a scattering problem, namely

$$\begin{cases} \Delta u_n + k^2 u_n = 0 \quad \text{in } S_0^+ = \{\mathbf{x} = (x_1, x_2) : x_2 > S_0(x_1)\}, \\ u_n(x_1, S_0(x_1)) = -\dfrac{F(x_1)^n}{n!}(-i\beta)^n \exp\left(i\alpha x_1 - i\beta S_0(x_1)\right) \\ \qquad\qquad\qquad\qquad - \displaystyle\sum_{m=0}^{n-1} \frac{F(x_1)^{n-m}}{(n-m)!} (\partial_y^{n-m} u_m)(x_1, S_0(x_1)), \\ u_n \text{ satisfies a radiation condition as } x_2 \to \infty. \end{cases} \tag{4}$$

As was shown in [24, 25] the analyticity results of [51] guarantee that expansions of increasing order do *converge* and, in fact, that they do so even beyond the radius of convergence of the series (3) provided the summation is suitably performed (e.g. through an appropriate use of conformal maps [24] or Padé approximation [25]).

2.2. A high-frequency integral equation method [17–19]

The boundary-variation methodology described above provides an efficient scattering solver that greatly improves on classical low-order methods based on shape perturbations and that, in fact, can outperform alternative state-of-the-art techniques [50, 53, 54]. As is the case with any such procedure however, the scheme described in §2.1, by itself, is of limited applicability at high frequencies (even if the function F is slowly oscillatory) as it demands the full resolution of the wavelength of radiation. As we have explained, these applications demand the use of different schemes that can explicitly account for the fast variations of the field. Classically these methods have relied on low-order asymptotic expansions, e.g. the Kirchhoff approximation, that possess their own limitations. Here we shall review some recently derived algorithms that avoid these limitations by resorting to high-order approximations. Just as the Kirchhoff approximation, these algorithms assume single-scattering configurations, that is the absence of shadowing and multiple scattering effects.

Specifically, we shall consider problems of the form (4) wherein the boundary data is highly oscillatory. More precisely, we seek solutions to

$$\begin{cases} \Delta u + k^2 u = 0 \quad \text{ in } S_0^+ = \{\mathbf{x} = (x_1, x_2) : x_2 > S_0(x_1)\}, \\ u(x_1, S_0(x_1)) = H(x_1)L(x_1), \\ u \text{ satisfies a radiation condition as } x_2 \to \infty. \end{cases} \tag{5}$$

where the functions H and L oscillate rapidly (i.e. on the scale of the wavelength of radiation $\lambda = 2\pi/k$) and slowly, respectively. For instance, the choice

$$H(x_1) = -\exp(i\alpha x_1 - i\beta S_0(x_1)) = \exp(ik\sin(\theta)x_1 - ik\cos(\theta)S_0(x_1)), \quad L(x_1) \equiv 1$$

would correspond to plane-wave incidence and is the case that was treated in [17–19]. The arguments in that work, however, readily apply to more general boundary data. Here, and with a view towards its use within the multi-scale solver we introduce below, we shall review these derivations as we extend the results in [19] to data of the form

$$H(x_1) = -\exp(ik\sin(\theta)x_1 - ik\cos(\theta)S_0(x_1) + ik\gamma x_1), \quad L(x_1) \equiv \sum_{n=-N}^{\infty} \nu_n(x_1)k^{-n} \tag{6}$$

for arbitrary fixed numbers γ and N and smooth functions ν_n; the original results in [19] correspond to $\gamma = N = 0$ and $\nu_n(x_1) \equiv 0$ for $n \geq 1$.

The starting point of the high-frequency solver is the integral-equation formulation of the scattering problem (5)-(6) wherein the field u is sought in the form of a single-layer potential

$$u(\mathbf{x}) = \int_{-\infty}^{\infty} \mu(x';\gamma;k) G_k(\mathbf{x};x') \sqrt{1+S_{0,x'}(x')^2}\, dx'$$

for an unknown surface density μ and where

$$G_k(\mathbf{x};x') = \frac{i}{4} H_0^{(1)}(kr),\ r = \sqrt{(x_1-x')^2+(x_2-S_0(x'))^2}$$

denotes the two-dimensional outgoing Green's function and $S_{0,x'}(x') = \dfrac{\partial S_0}{\partial x'}(x')$. The scattering problem (5)-(6) then is equivalent to the (first kind) integral equation [7]

$$\begin{aligned} &\frac{i}{4}\int_{-\infty}^{\infty} H_0^{(1)}(kr_0)\mu(x';\gamma;k)\sqrt{1+S_{0,x'}(x')^2}\, dx' \\ &\qquad = -\exp\left(ik\sin(\theta)x - ik\cos(\theta)S_0(x) + ik\gamma x\right)\sum_{n=-N}^{\infty}\nu_n(x)k^{-n} \end{aligned} \tag{7}$$

where $r_0 = \sqrt{(x-x')^2+(S_0(x)-S_0(x'))^2}$.

Our approach to the solution of equation (7) at high frequencies ($k \gg 1$) is based on a geometrical optics (GO) ansatz that factors out the rapid oscillations of the unknown density μ [7–11, 17–19, 55]. More precisely, we express the density as a slow, unknown modulation of an exponential which varies in-sync with the boundary data

$$\mu(x';\gamma;k) = \exp\left(ik\sin(\theta)x' - ik\cos(\theta)S_0(x') + ik\gamma x'\right)\mu^{\text{slow}}(x';\gamma;k). \tag{8}$$

In the absence of shadowing and multiple scattering effects, the validity of the phase extraction procedure (8) has been rigorously established in the literature [7–11, 17–19, 55]. This framework allows us to solve for the slowly varying envelope which, from (7) and (8), clearly satisfies

$$\begin{aligned} &\int_{-\infty}^{\infty}\exp\left[ik\left(\sin(\theta)(x'-x) - \cos(\theta)(S_0(x')-S_0(x)) + \gamma(x'-x)\right)\right] \\ &\qquad \times H_0^{(1)}(kr_0)\mu^{\text{slow}}(x';\gamma;k)\sqrt{1+S_{0,x'}(x')^2}\, dx' = 4i\sum_{n=-N}^{\infty}\nu_n(x)k^{-n}. \end{aligned} \tag{9}$$

To solve (9), and in the spirit of [17–19], we choose a series representations of the slowly varying envelope

$$\mu^{\text{slow}}(x';\gamma;k)\sqrt{1+S_{0,x'}(x')^2} = \sum_{n=-N-1}^{\infty}\mu_n(x';\gamma)k^{-n}, \tag{10}$$

consistent with the regularizing character of the single-layer potential. Using this representation, equation (9) can be written as

$$\sum_{n=-N-1}^{\infty} J_n(x;\gamma;k)k^{-n} = 4i \sum_{n=-N}^{\infty} \nu_n(x)k^{-n} \tag{11}$$

where

$$J_n(x;\gamma;k) = \int_{-\infty}^{\infty} \exp\left[ik\left(\sin(\theta)(x'-x) - \cos(\theta)(S_0(x') - S_0(x)) + \gamma(x'-x)\right)\right] \times H_0^{(1)}(kr_0)\mu_n(x';\gamma)\,dx'. \tag{12}$$

At this point we recognize that the functions J_n in (12) are given by oscillatory integrals, which can be evaluated asymptotically as $k \to \infty$ to any desired order. As in [17, 18], assuming the absence of shadowing effects, the values of these integrals are dominated by contributions from points x' in the vicinity of the "target point" x. To evaluate these contributions, we begin by separating the integral into $J_n = J_n^- + J_n^+$ where

$$J_n^-(x;\gamma;k) = \int_{-\infty}^{x} \exp\left[ik\left(\sin(\theta)(x'-x) - \cos(\theta)(S_0(x') - S_0(x)) + \gamma(x'-x)\right)\right] \times H_0^{(1)}(kr_0)\mu_n(x';\gamma)\,dx'.$$

$$J_n^+(x;\gamma;k) = \int_{x}^{\infty} \exp\left[ik\left(\sin(\theta)(x'-x) - \cos(\theta)(S_0(x') - S_0(x)) + \gamma(x'-x)\right)\right] \times H_0^{(1)}(kr_0)\mu_n(x';\gamma)\,dx'.$$

Equivalently, we can write

$$J_n^{\pm}(x;\gamma;k) = \int_{0}^{\infty} \exp\left[ik\left(\pm\sin(\theta)t - \cos(\theta)(S_0(x\pm t) - S_0(x)) \pm \gamma t\right)\right] \times H_0^{(1)}(k\phi^{\pm}(x,t))\mu_n(x\pm t,\gamma)\,dt \tag{13}$$

where $\phi^{\pm}(x,t) = \sqrt{t^2 + (S_0(x\pm t) - S_0(x))^2}$. Away from shadowing, the functions $u = \phi^{\pm}(x,\cdot)$ can be shown to be invertible [19] and therefore (13) can be written as

$$J_n^{\pm}(x;\gamma;k) = \int_0^{\infty} \widetilde{\mu}_n^{\pm}(x;u;\gamma)H_0^{(1)}(ku)\exp\left(-ik\psi_{\pm}(x;u;\gamma)\right)\,du$$

where

$$\widetilde{\mu}_n^{\pm}(x;u;\gamma) = \mu_n(x \pm (\phi^{\pm})^{-1}(x,u);\gamma)\left(\frac{d\phi^{\pm}}{dt}\left(x,(\phi^{\pm})^{-1}(x,u)\right)\right)^{-1} \quad \text{and}$$

$$\psi^{\pm}(x;u;\gamma) = (S_0(x \pm (\phi^{\pm})^{-1}(x,u)) - S_0(x))\cos(\theta) \mp (\phi^{+})^{-1}(x,u)(\sin(\theta)+\gamma).$$

Next, expanding $\widetilde{\mu}_n^{\pm}(x;u;\gamma)$ and $\psi^{\pm}(x;u;\gamma)$ in series in powers of u about $u = 0$ (corresponding to $x' = x$)

$$\widetilde{\mu}_n^{\pm}(x;u;\gamma) = \sum_{m=0}^{\infty} \widetilde{\mu}_{n,m}^{\pm}(x;\gamma)u^m, \quad \psi^{\pm}(x;u;\gamma) = \sum_{m=0}^{\infty} \psi_m^{\pm}(x;\gamma)u^m,$$

we find that

$$J_n^{\pm}(x;\gamma;k) = \sum_{q=0}^{\infty} \frac{J_{n,q}^{\pm}(x;\gamma)}{k^{q+1}}$$

with

$$J_{n,q}^{\pm}(x,\gamma) = \sum_{l=0}^{q} \widetilde{\mu}_{n,q-l}^{\pm}(x;\gamma) \left(\sum_{j=0}^{l} \frac{a_{j,l}^{\pm}(x;\gamma)}{j!} C^{\pm}(q+j;x;\gamma) \right)$$

and where the coefficients $a_{j,l}^{\pm}$ and $C^{\pm}$ are defined by

$$\left(i \sum_{l\geq 1} \psi_{l+1}^{\pm}(x;\gamma) u^l \right)^j = \sum_{l\geq j} a_{j,l}^{\pm}(x;\gamma) u^l$$

and

$$C^{\pm}(p;x;\gamma) = \int_0^{\infty} v^p H_0^{(1)}(v) e^{-i\psi_1^{\pm}(x;\gamma)v} dv.$$

Using obvious symmetries, we see that necessarily

$$\widetilde{\mu}_{n,m}^{-}(x;\gamma) = (-1)^m \widetilde{\mu}_{n,m}^{+}(x;\gamma), \quad \psi_l^{-}(x;\gamma) = (-1)^l \psi_l^{+}(x;\gamma) \quad \text{and} \quad a_{l,j}^{-}(x;\gamma) = (-1)^{l+j} a_{l,j}^{+}(x;\gamma),$$

and hence the complete asymptotic expansion of J^n takes on the explicit form

$$J_n(x;\gamma;k) = \sum_{q=0}^{\infty} \frac{J_{n,q}(x;\gamma)}{k^{q+1}} \tag{14}$$

with

$$J_{n,q}(x;\gamma) = \sum_{l=0}^{q} \widetilde{\mu}_{n,q-l}^{+}(x;\gamma) \left(\sum_{j=0}^{l} \frac{a_{j,l}^{+}(x;\gamma)}{j!} C(q+j;x;\gamma) \right) \tag{15}$$

and

$$C(q;x;\gamma) = \int_0^{\infty} v^q H_0^{(1)}(v) (e^{-i\psi_1^{+}(x;\gamma)v} + (-1)^p e^{i\psi_1^{+}(x;\gamma)v}) \, dv. \tag{16}$$

Expression (16) can be simplified if we use analytic continuation of moments of Hankel functions [56]

$$C(q;x;\gamma) = \begin{cases} 2^{q+1}\sum_{j=0}^{\infty} \frac{[2\psi_1^+(x;\gamma)]^{2j}}{(2j)!}(-1)^j \frac{\Gamma\left(\frac{q+2j+1}{2}\right)}{\Gamma\left(\frac{1-q-2j}{2}\right)} & \text{for } q \text{ even}, \\ -i2^{q+1}\sum_{j=0}^{\infty} \frac{[2\psi_1^+(x;\gamma)]^{2j+1}}{(2j+1)!}(-1)^j \frac{\Gamma\left(\frac{q+2j+2}{2}\right)}{\Gamma\left(\frac{-q-2j}{2}\right)} & \text{for } q \text{ odd}. \end{cases} \tag{17}$$

The series in (17) can be easily seen to be convergent for $|\psi_1^+(x;\gamma)| < 1$, and the values of $C(q;x;\gamma)$ can be explicitly computed as

$$C(q;x;\gamma) = C^{(q)}(\psi_1^+(x;\gamma))(1-\psi_1^+(x;\gamma)^2)^{-\frac{2q+1}{2}} \tag{18}$$

where $C^{(q)}$ are explicitly computable polynomials of degree q if q is even and $2[q/2]+1$ if q is odd; the first few are given by $C^{(0)}(x) = 2$, $C^{(1)}(x) = 2ix$, $C^{(2)}(x) = -2-4x^2$, and $C^{(3)}(x) = -18ix - 12ix^3$.

Finally, using the (14), (15) in (11) we derive the explicit recursion for the series coefficients μ_n in (10)

$$\mu_{-N-1}(x;\gamma) = \frac{4i\sqrt{1+S_{0,x}(x)^2}}{C(0;x;\gamma)}\ \nu_{-N}(x)$$

$$\mu_n(x;\gamma) = \frac{\sqrt{1+S_{0,x}(x)^2}}{C(0,x,\gamma)}\ \left[4i\nu_{n+1}(x) - \sum_{q=1}^{N+n+1}\left(\sum_{l=0}^{q}\widetilde{\mu}^+_{n-q,q-l}(x;\gamma) \times \sum_{j=0}^{l}\frac{a^+_{j,l}(x;\gamma)}{l!}C(q+j;x;\gamma)\right)\right],\ \text{for } n \geq -N,$$

where, from (18), the function $C(0;x;\gamma)$ is given by

$$C(0;x;\gamma) = \frac{2\sqrt{1+S_{0,x}(x)^2}}{(\cos^2\theta + S_{0,x}(x)^2\sin^2\theta + 2S_{0,x}(x)\cos\theta\sin\theta - \gamma^2 - 2\gamma\sin\theta + 2S_{0,x}(x)\gamma\cos\theta\sin\theta)^{\frac{1}{2}}}.$$

3. The multi-scale solver

In this section we present the details of our new multi-scale solver. As we have explained, the algorithm is based on a combination of the perturbative scheme described in §2.1 and the high-frequency method of §2.2. In §3.1 we derive the basic formulas that arise from this integration and which allow for the evaluation of scattering returns with arbitrary accuracy. As we show there, the scheme necessitates an extension of the high-frequency solver of §2.2 to allow for the stable calculation of the high-order derivatives of the field that arise

on application of the boundary-variation procedure of §2.1. In §3.2 we present method to enable such computations which is, again, based on integral representations and high-order asymptotic evaluation of oscillatory integrals.

3.1. The basic algorithm

Our approach relies on the use of a dichotomy in the frequency content of the scattering surface which amounts to viewing the original surface as a superposition of a component that contains small wavenumbers (relative to the wavenumber of the incident radiation), and thus is slowly oscillatory or "smooth", and a "rough" part comprised of the complementary, large wavenumbers. This decomposition is mathematically expressed as in (2) where S_0 and F correspond to the smooth and rough components respectively. The use of the boundary-variation procedure of §2.1 then reduces the original (multi-scale) problem (1) to the sequence of scattering problems (4) whose solutions can be found recursively. The fundamental property of these latter problems is that they are posed on a domain with a slowly varying boundary ($x_2 = S_0(x_1)$) and with *high-frequency* boundary data derived, by design, from the highly oscillatory nature of the rough component ($x_2 = F(x_1)$) of the surface (cf. (4)). As we show below, this characteristic allows, in this case, for the solution of the problems (4) to be effected through suitable extensions of the methods described in §2.2.

In detail, the first step in our approach is to choose a finite representation of the rapidly oscillatory component $F(x)$ in the form of a superposition of highly oscillatory exponentials

$$F(x) = \sum_{p=1}^{M} h_p e^{ik\gamma_p x} + \sum_{p=1}^{M} \bar{h}_p e^{-ik\gamma_p x}, \quad \text{with } \bar{h}_p = \pm h_p \tag{19}$$

in the spirit of the classical representation of the wavenumber spectrum of rough surfaces [7]. From (19), the powers of F then can be expressed using generalized binomial coefficients

$$F(x)^n = \sum_{p_1+\cdots+p_{2M}=n} \binom{n}{p_1,\cdots,p_{2M}} h_1^{p_1}\cdots h_M^{p_M}\bar{h}_1^{p_{M+1}}\cdots\bar{h}_M^{p_{2M}} \exp\left\{ik\left[\sum_{j=1}^{M}(p_j - p_{j+M})\gamma_j\right]x\right\}$$

and the recurrence (4) takes on the form

$$\begin{cases} \Delta u_n + k^2 u_n = 0 \quad \text{in } S_0^+ = \{\mathbf{x} = (x_1, x_2) : x_2 > S_0(x_1)\}, \\ u_n(x_1, S_0(x_1)) = -\dfrac{(-ik\cos(\theta))^n}{n!} \displaystyle\sum_{p_1+\cdots+p_{2M}=n} \binom{n}{p_1, \cdots, p_{2M}} h_1^{p_1} \cdots h_M^{p_M} \bar{h}_1^{p_{M+1}} \cdots \bar{h}_M^{p_{2M}} \\ \qquad \times \exp\left\{ ik \left[\Phi(x_1) + \left(\sum_{j=1}^{M} (p_j - p_{j+M})\gamma_j \right) x_1 \right] \right\} \\ \qquad - \displaystyle\sum_{m=0}^{n-1} \frac{1}{(n-m)!} \sum_{r_1+\cdots+r_{2M}=n-m} \binom{n-m}{r_1, \cdots, r_{2M}} h_1^{r_1} \cdots h_M^{r_M} \bar{h}_1^{r_{M+1}} \cdots \bar{h}_M^{r_{2M}} \\ \qquad \times \exp\left\{ ik \left(\displaystyle\sum_{j=1}^{M} (r_j - r_{j+M})\gamma_j \right) x_1 \right\} \frac{\partial^{n-m} u_m}{\partial y^{n-m}}(x_1, S_0(x_1)), \\ u_n \text{ satisfies a radiation condition as } x_2 \to \infty \end{cases} \tag{20}$$

where

$$\Phi(x) = \sin(\theta)x - \cos(\theta)S_0(x)$$

denotes the phase of the original incidence.

As described in §2.2, the application of the high-frequency method to the problems (20) requires the factorization of the boundary data into slow and fast oscillating components (cf. (5)). Now, from (20) it is easy to see (e.g. by induction and using the fact that the derivatives of u_m on the boundary must vary as u_m itself there, see §3.2) that

$$u_n(\mathbf{x}) = \sum_{p_1+\cdots+p_{2M}=n} u_{n,p_1,\cdots,p_{2M}}(\mathbf{x}) \tag{21}$$

where the functions $u_{n,p_1,\cdots,p_{2M}}(\mathbf{x})$ satisfy a scattering problem on S_0^+ with boundary data of the form

$$u_{n,p_1,\cdots,p_{2M}}(x, S_0(x)) = \exp\left\{ ik \left[\Phi(x) + \left(\sum_{j=1}^{M} (p_j - p_{j+M})\gamma_j \right) x \right] \right\} u^{\text{slow}}_{n,p_1,\cdots,p_{2M}}(x; k). \tag{22}$$

Moreover, the boundary values of the derivatives of $u_{n,p_1,\cdots,p_{2M}}(\mathbf{x})$ also possess a similar representation, which we write as

$$\frac{\partial^m u_{n,p_1,\cdots,p_{2M}}}{\partial y^m}(x, S_0(x)) = \exp\left\{ ik \left[\Phi(x) + \left(\sum_{j=1}^{M} (p_j - p_{j+M})\gamma_j \right) x \right] \right\} u^{\text{slow}}_{n,m,p_1,\cdots,p_{2M}}(x; k). \tag{23}$$

Thus, equation (20) can be thought of as providing a definition for the function $u^{\text{slow}}_{n,p_1,\cdots,p_{2M}} = u^{\text{slow}}_{n,0,p_1,\cdots,p_{2M}}$,

$$\begin{aligned} u^{\text{slow}}_{n,p_1,\cdots,p_{2M}}(x;k) = &-\frac{(-ik\cos(\theta))^n}{n!}\sum_{p_1+\cdots+p_{2M}=n}\binom{n}{p_1,\cdots,p_{2M}}h_1^{p_1}\cdots h_M^{p_M}\bar{h}_1^{p_{M+1}}\cdots\bar{h}_M^{p_{2M}} \\ &-\sum_{m=0}^{n-1}\frac{1}{(n-m)!}\sum_{r_1+\cdots+r_{2M}=n-m}\binom{n-m}{r_1,\cdots,r_{2M}} \\ &\times h_1^{r_1}\cdots h_M^{r_M}\bar{h}_1^{r_{M+1}}\cdots\bar{h}_M^{r_{2M}}u^{\text{slow}}_{m,n-m,p_1-r_1,\cdots,p_{2M}-r_M}(x;k). \end{aligned} \tag{24}$$

in terms of the functions $\left\{u^{\text{slow}}_{m,s,p_1,\cdots,p_{2M}}(x;k)\right\}_{m=0}^{n-1}$. In particular, if

$$u^{\text{slow}}_{m,s,p_1,\cdots,p_{2M}}(x;k) = \sum_{q=-(m+s)}^{\infty} u_{m,s,p_1,\cdots,p_{2M},q}(x)\ k^{-q} \quad \text{for } m \le n-1$$

it follows from (24) that

$$\begin{aligned} u_{n,p_1,\cdots,p_{2M},q}(x) = &-\delta_{n,q}\frac{(-i\cos(\theta))^n}{n!}\sum_{p_1+\cdots+p_{2M}=n}\binom{n}{p_1,\cdots,p_{2M}}h_1^{p_1}\cdots h_M^{p_M}\bar{h}_1^{p_{M+1}}\cdots\bar{h}_M^{p_{2M}} \\ &-\sum_{m=0}^{n-1}\frac{1}{(n-m)!}\sum_{r_1+\cdots+r_{2M}=n-m}\binom{n-m}{r_1,\cdots,r_{2M}} \\ &\times h_1^{r_1}\cdots h_M^{r_M}\bar{h}_1^{r_{M+1}}\cdots\bar{h}_M^{r_{2M}}u_{m,n-m,p_1-r_1,\cdots,p_{2M}-r_M,q}(x) \end{aligned} \tag{25}$$

where $\delta_{n,q}$ denotes the Kronecker delta.

The algorithm then can be inductively described as follows:

1. For $n = 0$, solve (20) using the high-frequency method as described in §2.2. The boundary data is simply given by

$$u_0(x, S_0(x)) = -\exp\left(ik\Phi(x)\right)$$

and

$$u^{\text{slow}}_{0,0,\cdots,0}(x;k) = -1.$$

As a result, we obtain a density $\mu_0^{\text{slow}} = \mu_0^{\text{slow}}(x;\gamma=0;k)$ and, from it, the complete solution

$$u_0(\mathbf{x}) = \int_{-\infty}^{\infty}\mu_0^{\text{slow}}(x';0;k)\exp\left[ik\Phi(x')\right]G_k(\mathbf{x};x')\sqrt{1+S_{0,x'}(x')^2}\,dx'.$$

2. Assume that the boundary data $u^{\text{slow}}_{m,p_1,\cdots,p_{2M}}(x;k) = u^{\text{slow}}_{m,0,p_1,\cdots,p_{2M}}(x;k)$ and the corresponding densities $\mu_m^{\text{slow}} = \mu_m^{\text{slow}}(x;\gamma=\sum_{j=1}^{M}(p_j-p_{j+M});k)$ have been computed

for $p_1 + \cdots + p_{2M} = m$ and $m < n$, where (cf. (21))

$$u_m(\mathbf{x}) = \sum_{p_1+\cdots+p_{2M}=m} u_{m,p_1,\cdots,p_{2M}}(\mathbf{x}) = \sum_{p_1+\cdots+p_{2M}=m} \int_{-\infty}^{\infty} \mu_m^{\text{slow}}(x'; \sum_{j=1}^{M}(p_j - p_{j+M}); k) \times \exp\left\{ ik \left[\Phi(x') + \left(\sum_{j=1}^{M}(p_j - p_{j+M}) \right) x' \right] \right\} G_k(\mathbf{x}; x') \sqrt{1 + S_{0,x'}(x')^2}\, dx'. \quad (26)$$

Then,

(a) Use the densities $\mu_m^{\text{slow}}(x; \sum_{j=1}^{M}(p_j - p_{j+M}); k)$ to find the derivatives $u^{\text{slow}}_{m,s,p_1,\cdots,p_M}(x; k)$, for $m < n, 0 < s$.

(b) From knowledge of $u^{\text{slow}}_{m,s,p_1,\cdots,p_M}(x; k)$, for $m < n$ and $0 < s$, use (24) to evaluate $u^{\text{slow}}_{n,p_1,\cdots,p_M}(x; k) = u^{\text{slow}}_{n,0,p_1,\cdots,p_M}(x; k)$ and (25) to find its expansion

$$u^{\text{slow}}_{n,0,p_1,\cdots,p_{2M}}(x; k) = \sum_{q=-n}^{\infty} u_{n,0,p_1,\cdots,p_{2M},q}(x)\ k^{-q} \quad (27)$$

in inverse powers of the wavenumber.

(c) For each fixed $p_1, \cdots, p_{2M}$ with $p_1 + \cdots + p_{2M} = n$, use (27) in (22) to define the (asymptotic expansion of the) boundary data for $u_{n,p_1,\cdots,p_{2M}}(\mathbf{x})$, and use the high-frequency algorithm to find the corresponding density $\mu_n^{\text{slow}}(x; \sum_{j=1}^{M}(p_j - p_{j+M}); k)$.

Note that **2.(b), (c)** deliver the values of $u^{\text{slow}}_{n,p_1,\cdots,p_M}(x; k)$ and $\mu_n^{\text{slow}}(x; \sum_{j=1}^{M}(p_j - p_{j+M}); k)$, respectively, which is precisely the information needed to proceed to the next iteration of step **2.**, and thus the algorithm is completely defined by this description. Moreover, this and the preceding discussions clearly delineate the details of each step, with the only exception of **2.(a)** which demands the calculation of high-order spatial derivatives of the successive solutions (cf. (23)). A procedure for the stable evaluation of these derivatives and of their complete asymptotic expansions is presented in the next section.

3.2. Calculation of the spatial derivatives

Our approach to the determination of the derivatives of the computed fields is based on the iterated calculation of the densities in their single-layer potential representation. More precisely, if the boundary values in (23) of the m-th derivative of a component $u_{n,p_1,\cdots,p_{2M}}$ are known together with the density entering its single-layer potential representation

$$\frac{\partial^m u_{n,p_1,\cdots,p_{2M}}}{\partial y^m}(x, S_0(x)) = \int_{-\infty}^{\infty} \mu_n^{m,\text{slow}}(x'; \sum_{j=1}^{M}(p_j - p_{j+M}); k) \times \exp\left\{ ik \left[\Phi(x') + \left(\sum_{j=1}^{M}(p_j - p_{j+M}) \right) x' \right] \right\} G_k(x, S_0(x); x') \sqrt{1 + S_{0,x'}(x')^2}\, dx' \quad (28)$$

we seek to evaluate the next order, $m+1$st, derivative and corresponding density, starting with $m=0$. In fact, we shall assume that we have found the high-frequency expansions (cf. (23))

$$\exp\left\{-ik\left[\Phi(x)+\left(\sum_{j=1}^{M}(p_j-p_{j+M})\gamma_j\right)x\right]\right\}\frac{\partial^m u_{n,p_1,\cdots,p_{2M}}}{\partial y^m}(x,S_0(x))$$
$$=u^{\text{slow}}_{n,m,p_1,\cdots,p_{2M}}(x;k)=\sum_{q=-(n+m)}^{\infty}u_{n,m,p_1,\cdots,p_{2M},q}(x)\;k^{-q} \quad (29)$$

and

$$\mu_n^{m,\text{slow}}(x';\sum_{j=1}^{M}(p_j-p_{j+M});k)=\sum_{q=-(n+m+1)}^{\infty}\mu_{n,m,p_1,\cdots,p_{2M},q}(x)\;k^{-q}$$

and shall derive similar representations for the functions $u^{\text{slow}}_{n,m+1,p_1,\cdots,p_{2M}}(x;k)$ and $\mu_n^{m+1,\text{slow}}(x';\sum_{j=1}^{M}(p_j-p_{j+M});k)$.

To evaluate $u^{\text{slow}}_{n,m+1,p_1,\cdots,p_{2M}}(x;k)$ we first note that

$$\frac{\partial^{m+1}u_{n,p_1,\cdots,p_{2M}}}{\partial y^{m}}(x,S_0(x))=\frac{\partial}{\partial y}\frac{\partial^m u_{n,p_1,\cdots,p_{2M}}}{\partial y^m}(x,S_0(x))$$
$$=n_2(x)\frac{\partial}{\partial\mathbf{n}}\frac{\partial^m u_{n,p_1,\cdots,p_{2M}}}{\partial y^m}(x,S_0(x))-n_1(x)\frac{\partial}{\partial\tau}\frac{\partial^m u_{n,p_1,\cdots,p_{2M}}}{\partial y^m}(x,S_0(x)) \quad (30)$$

where $\mathbf{n}=\mathbf{n}(x,S_0(x))=(n_1(x),n_2(x))$ and τ denote the normal and tangent vectors to the surface $x_2=S_0(x_1)$. Computing tangential derivatives is straightforward since, from (29),

$$\frac{\partial}{\partial\tau}\frac{\partial^m u_{n,p_1,\cdots,p_{2M}}}{\partial y^m} = \frac{d}{dx}\left(\exp\left\{ik\left[\Phi(x)+\left(\sum_{j=1}^{M}(p_j-p_{j+M})\gamma_j\right)x\right]\right\}\right.$$
$$\left.\times\sum_{q=-(n+m)}^{\infty} u_{n,m,p_1,\cdots,p_{2M},q}(x)\ k^{-q}\right).$$

The normal derivative of u, on the other hand, can be readily derived from the representation (28). Indeed, the classical jump relations for the derivatives of the single-layer potential imply that

$$\frac{\partial}{\partial\mathbf{n}}\frac{\partial^m u_{n,p_1,\cdots,p_{2M}}}{\partial y^m}(x,S_0(x)) =$$
$$-\frac{1}{2}\mu_n^{m,\mathrm{slow}}(x;\sum_{j=1}^{M}(p_j-p_{j+M});k)\sqrt{1+S_{0,x}(x)^2}\exp\left\{ik\left[\Phi(x)+\left(\sum_{j=1}^{M}(p_j-p_{j+M})\right)x\right]\right\}$$
$$+\int_{-\infty}^{\infty}\mu_n^{m,\mathrm{slow}}(x';\sum_{j=1}^{M}(p_j-p_{j+M});k)\exp\left\{ik\left[\Phi(x')+\left(\sum_{j=1}^{M}(p_j-p_{j+M})\right)x'\right]\right\}$$
$$\times\frac{\partial G_k}{\partial\mathbf{n}}(x,S_0(x);x')\sqrt{1+S_{0,x'}(x')^2}\,dx' \quad (31)$$

and the ideas of §2.2 can then be applied to determine the asymptotic expansion of the integral in the right-hand side of (31). In detail, letting this integral be denoted by $I_{n,m,p_1,\cdots,p_{2M}}(x;k)$, we have

$$I_{n,m,p_1,\cdots,p_{2M}}(x;k) = \exp\left\{ik\left[\Phi(x)+\left(\sum_{j=1}^{M}(p_j-p_{j+M})\right)x\right]\right\} I^{\mathrm{slow}}_{n,m,p_1,\cdots,p_{2M}}(x;k)$$

where

$$I^{\mathrm{slow}}_{n,m,p_1,\cdots,p_{2M}}(x;k) = \sum_{q=-(n+m)}^{\infty} I_{n,m,p_1,\cdots,p_{2M},q}(x)\ k^{-q}$$

and the coefficients $I_{n,m,p_1,\cdots,p_{2M},q}(x)$ can be determined recursively. Explicitly, as in the derivation of (15), the recursion reads

$$I_{n,m,p_1,\cdots,p_{2M},q}(x) = \frac{i}{4}\sum_{r=-(n+m)}^{q}\sum_{s=0}^{q-r}\widetilde{\mu}^{+}_{n,m,p_1,\cdots,p_{2M},r-1,q-r-s}(x)$$
$$\times\left(\sum_{j=0}^{s}\frac{a^{+}_{j,s}(x;\sum_{j=1}^{M}(p_j-p_{j+M}))}{j!}D(q+j-r;x;\sum_{j=1}^{M}(p_j-p_{j+M}))\right)$$

where

$$\widetilde{\mu}_{n,m,p_1,\cdots,p_{2M},q}(x) = \frac{\mu_{n,m,p_1,\cdots,p_{2M},q}(x)}{\sqrt{1+S_{0,x}(x)^2}},$$

$$g(x,x') = \frac{S_0(x) - S_0(x') - (x-x')S_{0,x}(x)}{(x'-x)^2 + (S_0(x') - S_0(x))^2},$$

$$g\left(x, x + (\phi^+)^{-1}(x,u)\right)\left(\frac{d\phi^+}{dt}\left(x, (\phi^+)^{-1}(x,u)\right)\right)^{-1} \widetilde{\mu}_{n,m,p_1,\cdots,p_{2M},q}\left(x + (\phi^+)^{-1}(x,u)\right)$$
$$= \sum_{m=0}^{\infty} \widetilde{\mu}^+_{n,m,p_1,\cdots,p_{2M},q,r}(x)u^r,$$

and the coefficients D are given by

$$D(p,x,\gamma) = \int_0^\infty v^{p+1} H_1^{(1)}(v)(e^{-i\psi_1^+(x,\gamma)v} + (-1)^p e^{i\psi_1^+(x,\gamma)v})dv.$$

Closed form formulas for the latter can be derived in a manner analogous to that used to obtain (17) and (18).

The above derivations deliver the asymptotic expansion of the $m+1$st derivative in (30) which, finally, we use to obtain the corresponding expansion for $\mu_n^{m+1,\text{slow}}$. To this end, we simply note that the latter is related to the (now, known) boundary values through a single-layer representation as in (28) (with m replaced by $m+1$), which we can view as an *integral equation* for the density $\mu_n^{m+1,\text{slow}}$ that can be solved with the high-frequency method of §2.2.

3.3. Truncation of the boundary perturbation series

We devote this subsection to certain remarks on the order of expansions that can be pursued in (3), which is precisely the number of problems of type (20) that need to be solved. Since the underlying high-frequency solver of our multiscale algorithm is applicable to single scattering configurations, both shadowing and multiple scattering effects impose restrictions on the number of terms in the boundary perturbation series (3) that can be pursued. Indeed, on one hand the convergence of the series in (18) requires that $|\psi_1^+(x,\gamma)| < 1$, which can be seen to be equivalent to the absence of shadowing. Thus, N terms can be kept in the expansion (18) provided that

$$\sin\theta + N\max\{|\gamma_j|,\ j = 1,\cdots,p\} < 1. \tag{32}$$

On the other hand, the phase extraction procedure (22) and the subsequent expansion of the slowly varying densities in inverse powers of k require that the only contribution in the asymptotic expansions of the oscillatory integrals in (26) comes from the target point

$x' = x$. This assumption rules out the existence of stationary points for the phases in (26), a condition that can be seen to be equivalent to

$$\sin\theta + \gamma - S_{0,x'}\cos\theta + \frac{x' - x + S_{0,x'}(S_0(x') - S_0(x))}{((x'-x)^2 + (S_0(x') - S_0(x))^2)^{\frac{1}{2}}} \neq 0 \tag{33}$$

for all x and x'. The previous condition (33) translates into a restriction on the number of terms in the series expansion (3) that can be kept. Indeed, in order to keep N terms in the perturbation series (3), the following condition must be further satisfied

$$\sin\theta + N\max\{|\gamma_j|,\ j = 1, \cdots, p\} - S_{0,x'}\cos\theta + \frac{x' - x + S_{0,x'}(S_0(x') - S_0(x))}{((x'-x)^2 + (S_0(x') - S_0(x))^2)^{\frac{1}{2}}} \neq 0 \tag{34}$$

for all x', x. In all the examples in the Numerical Results section we retained the maximum possible number of terms in the perturbation series according to the previous comments. As the number of terms retained typically depends on the wavelength of the incoming radiation and the curvature of the rough surfaces, we will illustrate in the next section the effect of these on the accuracy of our numerical scheme.

4. Numerical results

In this section we present numerical results of an application of the method described in the previous section to the treatment of periodic surfaces. As explained in §3.1 the overall scheme relies on the iterated evaluation of the slow envelopes μ_n^{slow} in (26) and of their derivatives which, in the periodic case, are themselves periodic. Thus, in this case, a spectral approach is particularly well-suited for the numerical realization of the procedure and we have therefore implemented a scheme based on representations on equispaced grids and on their dual Fourier expansions. For the repeated application of the high-frequency solver of §2.2 (to solve for μ_n^{slow} at each order, and to evaluate their spatial derivatives) we have followed the prescriptions delineated in [19] for the stable manipulation of "Taylor-Fourier series". The number N of terms that are kept in the perturbation series (3) is determined from the considerations related to shadowing and multiple scattering presented in §3.3.

For the results that follow we have considered scattering problems for the profiles (see Figure 1)

$$S_1^{(i)}(x) = S_0^{(i)}(x) + h_1\cos(50\pi x) = S_0^i(x) + F_1(x),\ i = 1, 2, 3 \tag{35}$$

and for the profiles

$$S_2^{(i)}(x) = S_0^{(i)} + h_1\cos(100\pi x) = S_0^{(i)}(x) + F_2(x),\ i = 1, 2, 3 \tag{36}$$

where the functions $S_0^{(i)}$ are defined as

$$S_0^{(1)}(x) = \frac{h}{2}\cos(2\pi x)$$

$$S_0^{(2)}(x) = \frac{h}{2}(\cos(2\pi x) + \cos(4\pi x))$$

$$S_0^{(3)}(x) = \frac{h}{2}(-\cos(2\pi x) + 0.35\cos(4\pi x) - 0.035\cos(6\pi x))$$

so that the profiles can be considered to be periodic with period $d = 1$.

The first set of results, in Tables 1–3, consist of scattering experiments for the profiles (35) under normal incidence with wavelength $\lambda = 0.00204$ and a comparable height $h = 0.001$. The small scale features here are of the form (19) with $M = 1$ and $\gamma_1 = 0.051$, and their size was set to $h_1 = 0.0004$. The tables display the relative errors incurred by our approximation scheme in computing the energy e_r scattered in some representative directions ($0 \le r \le 5$); the r-th order "efficiency" e_r is defined as [57]

$$e_r = \frac{|B_r|^2\beta_r}{\beta}$$

where B_r is the amplitude of the wave scattered in the direction

$$(\alpha_r, \beta_r) = (\alpha + (2\pi/d)r, \sqrt{k^2 - \alpha_r^2}) = (k\cos(\theta_r), k\cos(\theta_r))\,, \tag{37}$$

that is,

$$u(\mathbf{x}) = \sum_{r=-\infty}^{\infty} B_r\ \exp\left(i\alpha_r x_1 + i\beta_r x_2\right) \quad \text{for } x_2 > S_j^{(i)}(x_1).$$

Each table caption also includes the value of the defect in energy balance

$$\epsilon = |1 - \sum_{r \text{ propagating}} e_r|,$$

incurred at the last displayed order of summation, which can be interpreted as providing a certain measure of the accuracy of the remaining propagating modes (i.e. those for which $k^2 \ge \alpha_r^2$) that are not displayed.

The tables show the errors that arise on using approximations to (3) obtained by retaining $1, 4, 8, 12$ and 19 terms in the expansion computed from (20) as described in §3.1. We note

Table 1. Results for the profile (35), $i = 1$, with $h = 0.001$, $h_1 = 0.0004$, $\lambda = 0.00204$, $\theta = 0^o$, $\epsilon = 1.8e-10$.

Efficiency	Scattered energy	Order 0	Order 3	Order 7	Order 11	Order 18
0	0.7125785050439515e-04	1.14e+03	3.04e+02	6.70e-01	1.54e-03	3.25e-10
1	0.8302078889595598e-04	1.15e+03	3.04e+02	6.70e-01	1.53e-03	1.28e-10
2	0.2060899176821211e-03	1.15e+03	3.04e+02	6.71e-01	1.54e-03	1.30e-10
3	0.9084840392300477e-04	1.15e+03	3.05e+02	6.71e-01	1.53e-03	5.05e-10
4	0.1775672463729350e-04	1.14e+03	3.05e+02	6.70e-01	1.54e-03	1.06e-09
5	0.2005842496375083e-05	1.15e+03	3.05e+02	6.71e-01	1.53e-03	1.80e-09

Table 2. Results for the profile (35), $i = 2$, with $h = 0.001$, $h_1 = 0.0004$, $\lambda = 0.00204$, $\theta = 0^o$, $\epsilon = 3.9e-10$.

Efficiency	Scattered energy	Order 0	Order 3	Order 7	Order 11	Order 18
0	0.7703719607123411e-04	1.14e+03	3.04e+02	6.70e-01	1.54e-03	3.37e-10
1	0.2085591998781614e-05	1.15e+03	3.04e+02	6.69e-01	1.53e-03	3.74e-09
2	0.1330672394083418e-03	1.14e+03	3.04e+02	6.70e-01	1.54e-03	2.42e-10
3	0.4201899407415448e-04	1.15e+03	3.05e+02	6.71e-01	1.54e-03	3.12e-09
4	0.1226934955328155e-04	1.14e+03	3.03e+02	6.68e-01	1.53e-03	1.41e-09
5	0.7292080782334352e-04	1.14e+03	3.03e+02	6.69e-01	1.53e-03	2.30e-09

that 19 is the maximum number of terms that can be retained in the boundary perturbation series according to the results in §3.3. At each stage of the recursion the expansion (27) of (the slow envelopes of) the boundary data (22) was approximated by retaining only 6 terms. More precisely, at the n-th stage of the recurrence, the series in k^{-1} were taken from $-n$ to $6-n$ for the calculation of $u^{\rm slow}_{n,p_1,\cdots,p_{2M}}$, from $-m-n$ to $6-m-n$ for $u^{\rm slow}_{n,m,p_1,\cdots,p_{2M}}$, and from $-1-n$ to $5-n$ for $\mu^{\rm slow}_n$; the decision to effect the truncation at these orders stems from extensive experimentation, which suggests that (here, and in the examples that follow) the use of higher order expansions translates into only minimal accuracy gains.

The errors were calculated using a reference solution obtained from an application of the high-order perturbative method of §2.1 to the solution of the full problem (that is, with $S_0^{(i)}$ replaced by $S_1^{(i)}$) which, in this case, can be shown to provide answers with double precision accuracy. The tables clearly show the beneficial effect of high-order approximations. In fact, the relative large size of the small-scale perturbations, which here reach 80% of the height of the underlying long-scale surfaces, result in low-order approximations with no accuracy at all.

Similar results can be obtained for the more oscillatory profiles (36), even if the amplitude of the rapidly oscillatory component of the surface is decreased to $h_1 = 0.0002$ (see Figure 1). In tables 4-6 we present results corresponding to each of the three instances of this type of

Table 3. Results for the profile (35), $i = 3$, with $h = 0.001$, $h_1 = 0.0004$, $\lambda = 0.00204$, $\theta = 0^o$, $\epsilon = 3.8e-10$.

Efficiency	Scattered energy	Order 0	Order 3	Order 7	Order 11	Order 18
0	0.2321315509610210e-03	1.15e+03	3.04e+02	6.70e-01	1.54e-03	3.25e-10
1	0.5614717586397124e-04	1.14e+03	3.04e+02	6.70e-01	1.53e-03	1.01e-10
2	0.8281482315464451e-04	1.15e+03	3.04e+02	6.71e-01	1.54e-03	6.14e-10
3	0.9098525464968133e-04	1.15e+03	3.05e+02	6.71e-01	1.53e-03	2.88e-10
4	0.5586539410176244e-04	1.15e+03	3.04e+02	6.71e-01	1.54e-03	4.04e-10
5	0.2326632299430769e-04	1.15e+03	3.05e+02	6.71e-01	1.54e-03	1.38e-09

Table 4. Results for the profile (36), $i = 1$, with $h = 0.001$, $h_1 = 0.0002$, $\lambda = 0.00102$, $\theta = 0^o$, $\epsilon = 3.9e-10$.

Efficiency	Scattered energy	Order 0	Order 3	Order 7	Order 11	Order 18
0	0.3220194019274500e-04	1.15e+03	3.04e+02	6.70e-01	1.53e-03	2.99e-10
1	0.5117382229887928e-04	1.14e+03	3.05e+02	6.47e-01	1.54e-03	2.39e-10
2	0.6395079226503710e-04	1.16e+03	3.04e+02	6.71e-01	1.54e-03	3.75e-10
3	0.3843679338877258e-05	1.15e+03	3.04e+02	6.70e-01	1.58e-03	7.25e-10
4	0.9811658223497998e-04	1.14e+03	3.05e+02	6.48e-01	1.51e-03	1.44e-10
5	0.1188681563981649e-03	1.14e+03	3.04e+02	6.70e-01	1.60e-03	2.97e-10

surface, illuminated at a higher frequency ($\lambda = 0.00102$) so as to retain the same value for the ratio h_1/λ and for $\gamma_1 = 0.051$ as in the previous examples.

The next set of results, in tables 7–12, concern scattering experiments for the six profiles under oblique incidence, $\theta = 30^o$. Here, the size of the fast oscillations and the wavelength were chosen so as to maintain the same level of roughness as in the previous experiments as measured by the Rayleigh parameter $h_1 \cos\theta/\lambda$. Again, the reference solutions were produced by direct implementations of the method of variations of boundaries of §2.1 whenever this

Table 5. Results for the profile (36), $i = 2$, with $h = 0.001$, $h_1 = 0.0002$, $\lambda = 0.00102$, $\theta = 0^o$, $\epsilon = 4.8e-10$.

Efficiency	Scattered energy	Order 0	Order 3	Order 7	Order 11	Order 18
0	0.6921078334453966e-04	1.15e+03	3.04e+02	6.70e-01	1.54e-03	8.59e-09
1	0.4081769864172771e-05	1.14e+03	3.05e+02	6.70e-01	1.54e-03	2.08e-07
2	0.1584856041118052e-04	1.14e+03	3.04e+02	6.70e-01	1.53e-03	1.62e-07
3	0.5751503076918858e-05	1.14e+03	3.04e+02	6.70e-01	1.64e-03	8.24e-08
4	0.5766846771318473e-04	1.14e+03	3.04e+02	6.70e-01	1.53e-03	3.08e-08
5	0.3564528238052267e-04	1.14e+03	3.04e+02	6.70e-01	1.54e-03	3.79e-09

Table 6. Results for the profile (36), $i = 3$, with $h = 0.001$, $h_1 = 0.0002$, $\lambda = 0.00102$, $\theta = 0^o$, $\epsilon = 5.8e-10$.

Efficiency	Scattered energy	Order 0	Order 3	Order 7	Order 11	Order 18
0	0.1723266914079195e-03	1.14e+03	3.04e+02	6.70e-01	1.52e-03	1.52e-10
1	0.5118549971262311e-04	1.15e+03	3.04e+02	6.70e-01	1.54e-03	3.38e-10
2	0.6144808283856077e-04	1.14e+03	3.05e+02	6.71e-01	1.55e-03	3.87e-10
3	0.2860834316644127e-04	1.14e+03	3.04e+02	6.70e-01	1.64e-03	3.76e-10
4	0.2267246175277595e-05	1.14e+03	3.04e+02	6.69e-01	1.54e-03	1.62e-09
5	0.1690514661574384e-04	1.14e+03	3.04e+02	6.70e-01	1.65e-03	1.22e-09

Table 7. Results for the profile (35), $i = 1$, with $h = 0.001$, $h_1 = 0.0002$, $\lambda = 0.00102$, $\theta = 30^o$, $\epsilon = 1.9e-11$.

Efficiency	Scattered energy	Order 0	Order 3	Order 7	Order 11	Order 18
0	0.8885549833399981e-04	4.48e+01	1.31e-01	3.72e-02	5.53e-05	4.50e-13
1	0.2630310908320908e-02	4.45e+01	1.46e-01	3.70e-02	5.49e-05	3.89e-12
2	0.9270391685422687e-04	4.42e+01	1.60e-01	3.68e-02	5.45e-05	5.33e-11
3	0.1970560010679330e-02	4.40e+01	1.74e-01	3.66e-02	5.41e-05	1.16e-11
4	0.3565510968529941e-02	4.37e+01	1.88e-01	3.64e-02	5.38e-05	9.28e-13
5	0.2041506981776900e-02	4.35e+01	2.02e-01	3.62e-02	5.34e-05	8.09e-12

could be trusted to produce very accurate results. This was actually the case for every one of these experiments except for those in Tables 11 and 12; for these the accuracy that is attainable with a direct application of this procedure cannot exceed single precision. This is due to the increased complexity of these latter configurations, which can translate into cancellation errors within numerical procedures based solely on shape deformation [38, 39]. In fact, the complex nature of these geometrical arrangements, coupled to the high frequency of oscillation of the incident radiation, presents significant challenges for *every* alternative state-of-the-art solver (e.g. that in [2], with which we compare other results below), and it renders these unable to resolve the problem in practical computational times. For this reason the errors presented in Tables 11 and 12 were computed in relation to a highly resolved solution (Order 18) as produced by the current multi-scale method. In the latter case, and for comparison, we also include in Table 13 the errors obtained when compared to a direct solution via boundary variations (cf. §2.1) which, in this case, can be only guaranteed to possess 7 digits of accuracy.

In tables 14–16 we present results for more complex profiles, namely

$$S_3^{(i)}(x) = S_0^{(i)} + h_1(\cos(50\pi x) + \cos(100\pi x)) = S_0^{(i)}(x) + F_3(x),\ i = 1, 2, 3. \quad (38)$$

wherein the high-frequency component contains more than one scale. The results correspond

Table 8. Results for the profile (35), $i = 2$, with $h = 0.001$, $h_1 = 0.0002$, $\lambda = 0.00102$, $\theta = 30^o$, $\epsilon = 7.2e-11$.

Efficiency	Scattered energy	Order 0	Order 3	Order 7	Order 11	Order 18
0	0.2196490278049946e-03	3.98e+01	3.03e-01	3.53e-02	5.24e-05	2.08e-10
1	0.5082460374969916e-03	4.77e+01	3.07e-02	3.82e-02	5.68e-05	1.53e-09
2	0.1421290694952387e-02	4.20e+01	2.38e-01	3.60e-02	5.32e-05	4.70e-10
3	0.3629288948636560e-03	5.05e+01	7.65e-02	3.88e-02	5.74e-05	1.79e-09
4	0.2524857334133189e-03	6.63e+01	7.09e-01	4.35e-02	6.46e-05	1.76e-09
5	0.3386699737820342e-02	3.63e+01	4.26e-01	3.32e-02	4.88e-05	2.94e-10

Table 9. Results for the profile (35), $i = 3$, with $h = 0.001$, $h_1 = 0.0002$, $\lambda = 0.00102$, $\theta = 30^o$, $\epsilon = 1.9e-11$.

Efficiency	Scattered energy	Order 0	Order 3	Order 7	Order 11	Order 18
0	0.1999444889329398e-02	4.48e+01	1.32e-01	3.73e-02	5.53e-05	1.40e-11
1	0.3482870139291976e-02	4.45e+01	1.46e-01	3.71e-02	5.49e-05	1.95e-12
2	0.9312287660659891e-03	4.43e+01	1.60e-01	3.69e-02	5.46e-05	1.40e-11
3	0.4426354000069988e-04	4.40e+01	1.75e-01	3.67e-02	5.42e-05	2.01e-10
4	0.5340069488986556e-03	4.38e+01	1.89e-01	3.65e-02	5.38e-05	5.20e-11
5	0.1410308180715168e-02	4.35e+01	2.03e-01	3.63e-02	5.34e-05	3.24e-11

Table 10. Results for the profile (36), $i = 1$, with $h = 0.001$, $h_1 = 0.0001$, $\lambda = 0.00051$, $\theta = 30^o$, $\epsilon = 1.9e-11$.

Efficiency	Scattered energy	Order 0	Order 3	Order 7	Order 11	Order 18
0	0.1057625632013217e-02	4.48e+01	1.31e-01	3.73e-02	5.53e-05	2.06e-10
1	0.2930030362936720e-03	4.46e+01	1.39e-01	3.72e-02	5.51e-05	9.96e-10
2	0.8684902826984089e-03	4.45e+01	1.46e-01	3.70e-02	5.49e-05	1.24e-09
3	0.7916708314714082e-03	4.44e+01	1.53e-01	3.69e-02	5.47e-05	4.74e-10
4	0.1904719643869867e-03	4.43e+01	1.60e-01	3.68e-02	5.45e-05	2.79e-09
5	0.1486308594726963e-02	4.41e+01	1.67e-01	3.67e-02	5.44e-05	4.51e-10

Table 11. Results for the profile (36), $i = 2$, with $h = 0.001$, $h_1 = 0.0001$, $\lambda = 0.00051$, $\theta = 30^o$, $\epsilon = 1.9e-11$.

Efficiency	Scattered energy	Order 0	Order 3	Order 7	Order 11	Order 17
0	0.4516187423114953e-03	4.48e+01	1.32e-01	3.73e-02	5.53e-05	3.28e-10
1	0.2027235633240862e-03	4.47e+01	1.37e-01	3.71e-02	5.52e-05	3.27e-10
2	0.2279372386925942e-03	4.45e+01	1.48e-01	3.70e-02	5.49e-05	3.25e-10
3	0.7643647924649606e-03	4.44e+01	1.53e-01	3.69e-02	5.47e-05	3.24e-10
4	0.2582220221076261e-03	4.43e+01	1.59e-01	3.68e-02	5.46e-05	3.22e-10
5	0.4690562318953122e-03	4.42e+01	1.67e-01	3.67e-02	5.44e-05	3.21e-10

Table 12. Results for the profile (36), $i = 3$, with $h = 0.001$, $h_1 = 0.0001$, $\lambda = 0.00051$, $\theta = 30^o$, $\epsilon = 6.3e-11$. Errors computed with respect to a highly resolved solution (Order 18) obtained with the present scheme.

Efficiency	Scattered energy	Order 0	Order 3	Order 7	Order 11	Order 17
0	0.2024725121616445e-02	4.48e+01	1.31e-01	3.72e-02	5.53e-05	3.28e-10
1	0.2558417218609767e-02	4.46e+01	1.38e-01	3.71e-02	5.51e-05	3.27e-10
2	0.2078244901063298e-03	4.45e+01	1.46e-01	3.70e-02	5.50e-05	3.25e-10
3	0.4709095153227742e-03	4.44e+01	1.53e-01	3.69e-02	5.47e-05	3.24e-10
4	0.7539238536010719e-03	4.42e+01	1.60e-01	3.68e-02	5.46e-05	3.22e-10
5	0.1366988401673538e-03	4.41e+01	1.67e-01	3.67e-02	5.44e-05	3.21e-10

Table 13. Results for the profile (36), $i = 3$, with $h = 0.001$, $h_1 = 0.0001$, $\lambda = 0.00051$, $\theta = 30^o$, $\epsilon = 6.3e-11$. Errors computed with respect to a solution obtained from a direct application of the method of variation of boundaries of §2.1.

Efficiency	Scattered energy	Order 0	Order 3	Order 7	Order 11	Order 18
0	0.20247256e-02	4.48e+01	1.31e-01	3.72e-02	5.56e-05	2.79e-07
1	0.25584178e-02	4.46e+01	1.38e-01	3.71e-02	5.53e-05	2.49e-07
2	0.20782455e-03	4.45e+01	1.46e-01	3.70e-02	5.52e-05	3.34e-07
3	0.47090996e-03	4.44e+01	1.53e-01	3.69e-02	5.57e-05	9.52e-07
4	0.75392400e-03	4.42e+01	1.60e-01	3.68e-02	5.47e-05	1.95e-07
5	0.13669892e-03	4.41e+01	1.67e-01	3.67e-02	5.49e-05	5.85e-07

to $h = 0.001$, $h_1 = 0.0001$, $\lambda = 0.00102$ and $M = 2$, $\gamma_1 = 0.0255$ and $\gamma_2 = 0.0510$ in (19); the reference solution is again that provided by direct application of the high-order perturbative method described in §2.1. Again here we see that high-order expansions are necessary to attain accurate solutions.

The next set of results in Figure 2 present the performance of our algorithm with respect to the number of terms that can be retained in the boundary perturbation series (3) so

Table 14. Results for the profile (38) with $i = 1$, $h = 0.001$, $h_1 = 0.0001$, $\lambda = 0.00102$, $\theta = 0^o$, $\epsilon = 1.7e-08$.

Efficiency	Scattered energy	Order 0	Order 3	Order 6	Order 9	Order 12
0	0.7809673857438551e-02	3.73e+00	4.65e-01	2.54e-02	6.32e-04	3.02e-06
1	0.1241103893438373e-01	3.73e+00	4.65e-01	2.54e-02	6.32e-04	3.02e-06
2	0.1551086664560946e-01	3.73e+00	4.65e-01	2.54e-02	6.33e-04	3.02e-06
3	0.9323641198672753e-03	3.73e+00	4.65e-01	2.54e-02	6.33e-04	3.03e-06
4	0.2380403565078734e-01	3.73e+00	4.65e-01	2.54e-02	6.32e-04	3.01e-06
5	0.2884446608927802e-01	3.73e+00	4.65e-01	2.54e-02	6.32e-04	3.03e-06

Table 15. Results for the profile (38) with $i = 2$, $h = 0.001$, $h_1 = 0.0001$, $\lambda = 0.00102$, $\theta = 0^o$, $\epsilon = 2.4e-08$.

Efficiency	Scattered energy	Order 0	Order 3	Order 6	Order 9	Order 12
0	0.1620350090640221e-01	3.90e+00	4.85e-01	2.58e-02	6.81e-04	1.50e-05
1	0.9807023136707068e-03	3.78e+00	3.70e-01	2.95e-02	5.20e-04	3.84e-05
2	0.3593958390013861e-02	4.06e+00	5.30e-01	2.49e-02	6.97e-04	6.50e-05
3	0.1914610747999278e-02	2.45e+00	3.50e-01	1.86e-02	4.04e-04	1.98e-05
4	0.1578480386178771e-01	3.19e+00	3.77e-01	2.45e-02	4.65e-04	5.07e-05
5	0.1052572875412128e-01	2.89e+00	5.78e-01	1.21e-02	6.93e-04	2.42e-05

Table 16. Results for the profile (38) with $i = 3$, $h = 0.001$, $h_1 = 0.00011$, $\lambda = 0.00102$, $\theta = 0^o$,$\epsilon = 1.8e-08$.

Efficiency	Scattered energy	Order 0	Order 3	Order 6	Order 9	Order 12
0	0.4179247717389074e-01	3.73e+00	4.65e-01	2.54e-02	6.35e-04	2.51e-05
1	0.1241412009345886e-01	3.73e+00	4.65e-01	2.54e-02	6.33e-04	2.65e-05
2	0.1490315383075556e-01	3.73e+00	4.65e-01	2.54e-02	6.24e-04	3.56e-05
3	0.6941016570048612e-02	3.73e+00	4.65e-01	2.53e-02	6.31e-04	2.84e-05
4	0.5494977435238026e-03	3.74e+00	4.64e-01	2.54e-02	6.73e-04	1.44e-05
5	0.4109507007508514e-02	3.72e+00	4.66e-01	2.53e-02	6.02e-04	5.75e-05

that the high-frequency component of our multiscale solver is applicable. More precisely, we present the dependence of the relative error in the backscattered energy (i.e. $e_{0,0}$) on the ratio λ/R, where λ is the wavelength of the incoming radiation and R is the maximum radius of the curvature of the rough surface. In all these examples, 6 terms were used in the k^{-1} series. The reference solutions were produced in all cases by direct application of the high-order perturbative method described in §2.1. The multiscale configurations in Figure 2 range from cases where the radius of the curvature is about 44 wavelength to cases where the radius of curvature is 3 wavelength. Specifically, we considered examples for the profiles (36) for $i = 3$ under normal incidence with $h = 0.002$ and the following choices of λ and h_1: (1) $\lambda = 0.0015$ and $h_1 = 0.00015$; (2) $\lambda = 0.0015$ and $h_1 = 0.00019$; (3) $\lambda = 0.0015$ and $h_1 = 0.00025$; (4) $\lambda = 0.0021$ and $h1 = 0.00025$; (5) $\lambda = 0.0021$ and $h_1 = 0.00035$; (6) $\lambda = 0.0027$ and $h_1 = 0.00034$; (7) $\lambda = 0.0035$ and $h_1 = 0.00035$; (8) $\lambda = 0.0035$ and $h_1 = 0.00039$; (9) $\lambda = 0.0035$ and $h_1 = 0.00045$; (10) $\lambda = 0.004$ and $h_1 = 0.0005$; (11) $\lambda = 0.0045$ and $h_1 = 0.00055$; (12) $\lambda = 0.0047$ and $h_1 = 0.0006$; and (13) $\lambda = 0.0049$ and $h_1 = 0.00068$. Results of a similar quality were obtained for the same type of profiles for $i = 1, 2$. The number of terms in the perturbation series (3) is directly proportional to the quotient λ/R (14 terms were returned for case (1), 12 terms for (2), 11 terms for (3), 8 terms for (4), 7 terms for (5), 6 terms for (6), 5 terms for (7) and (8), and 4 terms for (9)-(13) respectively) and consequently the quality of the approximation of our algorithm

Table 17. Results for the profile (35), $i = 3$, with $h = 0.02$, $h_1 = 0.0002$, $\lambda = 0.00102$, $\theta = 30^o$, $\epsilon = 8.3e - 10$.

Efficiency	Scattered energy	KA	Order 0	Order 5
0	0.3974638875106871e-02	1.18e-04	1.63e-08	2.66e-10
1	0.4610686287732108e-02	4.93e-06	2.09e-07	4.40e-10
2	0.1605727590442480e-02	7.66e-05	5.95e-08	1.87e-10
3	0.1377763310395526e-01	1.65e-05	5.58e-08	1.61e-10
3	0.1377763310395526e-01	6.33e-05	3.35e-07	5.31e-10
5	0.5367076168190201e-02	4.94e-05	2.18e-08	1.85e-10

is conditioned by the number of terms retained. For comparison purposes it must be noted that the classical two-scale method typically retains at most two terms both in the boundary perturbation series as well as in the series in the inverse powers of the wavenumber.

We illustrate in Table 17 a convergence study in terms of the number of terms in inverse powers k retained in all expansions (27) of (the slow envelopes of) the boundary data (22). As previously described, we have retained 6 terms in all the series in k^{-1} for the calculation of μ_n^{slow}. For the case presented in Table 17, we added all 17 terms in the boundary perturbation series and the results as we increase the number of terms in the k series expansions of the data (22), from one term (Order -1 that corresponds to the Kirchhoff Approximation (KA)) to 6 terms (Order 5). The reference solution was obtained through the application of the current algorithm of order 18 in the boundary perturbation series.

The next set of tables, tables 18–20, correspond to examples where the height-to-wavelength ratio h/λ is significantly increased with respect to the previous cases. Specifically, we consider the profiles (35) where the parameters h are taken to be those from the examples in [19]. The wavelength is fixed at $\lambda = 0.00204$, resulting in height-to-wavelength ratios of approximately 12.25, 4.9 and 9.8 for $i = 1, 2$ and 3, respectively; the height of the rapidly oscillatory function F_1 is $h_1 = 0.0004$, and the incidence is normal. These configurations lie outside of the domain where solutions based on direct application of the method of §2.1 are accurate, and therefore our reference solutions were produced with an alternative approach. This recently derived approach [2] is based on a novel procedure for the fast and accurate solution of the integral equation formulation of the scattering problem (1); the scheme relies on techniques that accelerate the (slow) convergence of the periodized Green's function while still allowing for its accurate computation, and on high-order quadrature rules that are well-adapted to the evaluation of the resulting integrals. The comparison with this method, which is perhaps the most advanced rigorous solver that has been developed to date, highlights the benefits of our proposed strategy for the treatment of multi-scale surfaces. Indeed, even in these rather moderate examples, the computational times of a most straightforward implementation of our new procedure entail only a small fraction (of approximately 1/56) of that necessary to

Table 18. Results for the profile (35), $i = 1$, with $h = 0.025$, $h_1 = 0.0004$, $\lambda = 0.00204$, $\theta = 0^o$, $\epsilon = 3.5e-09$.

Efficiency	Scattered energy	Order 0	Order 3	Order 7	Order 11	Order 17
0	0.7318582656363349e-04	5.22e+01	2.45e+02	5.06e-01	1.10e-03	1.53e-08
1	0.7367172206066630e-02	3.99e-01	2.14e-01	8.87e-03	2.85e-05	9.38e-09
2	0.1402077277268780e-01	7.37e-01	5.42e-01	9.72e-03	2.53e-05	1.73e-09
3	0.1875966512975140e-02	1.58e+00	6.62e+00	6.63e-02	1.73e-04	2.25e-08
4	0.9770168586492420e-03	2.13e+00	8.63e-01	5.67e-03	6.49e-06	1.37e-08
5	0.4898861375663570e-02	1.58e-01	3.82e+00	4.88e-02	1.32e-04	7.13e-09

Table 19. Results for the profile (35), $i = 2$, with $h = 0.01$, $h_1 = 0.0004$, $\lambda = 0.00204$, $\theta = 0^o$, $\epsilon = 3.6e-09$.

Efficiency	Scattered energy	Order 0	Order 3	Order 7	Order 11	Order 17
0	0.7177866272135938e-02	8.13e-01	5.61e-01	1.46e-02	4.44e-05	5.50e-09
1	0.7380037563008497e-02	8.64e-01	7.63e-02	5.43e-03	1.79e-05	4.34e-09
2	0.6452135098915328e-02	2.61e-01	1.21e+00	1.20e-02	3.98e-05	1.09e-08
3	0.4915495200946559e-03	1.54e+01	9.15e-01	1.82e-02	6.35e-05	9.90e-09
4	0.2250692885973962e-03	2.76e+01	8.80e+00	5.90e-03	1.81e-05	1.03e-08
5	0.2594523160923045e-02	4.43e-01	1.21e+00	1.33e-02	3.33e-05	1.41e-08

produce comparably accurate solutions with the methodology of [2].

Finally, in Figure 3 we further exemplify the multi-scale effects in the solution of the scattering problems (1). The figure displays the far-field data for the configurations of tables 18–20 (gray outer curves) together with that corresponding to the same arrangement but with the multi-scale profiles replaced by their low-frequency, smooth components S_0^i, $i = 1, 2, 3$ (black inner curves; cf. Figure 1(a)-(c)). More precisely, the figure shows the polar plots of the efficiencies e_r corresponding to the propagating directions $\theta_r = \tan^{-1}(\beta_r/\alpha_r)$

Table 20. Results for the profile (35), $i = 3$, with $h = 0.02$, $h_1 = 0.0004$, $\lambda = 0.00204$, $\theta = 0^o$, $\epsilon = 9.2e-08$.

Efficiency	Scattered energy	Order 0	Order 3	Order 7	Order 11	Order 17
0	0.3546428035456250e-02	1.99e+01	6.03e+00	4.82e-02	1.28e-04	2.95e-09
1	0.4028515289161730e-02	1.09e+01	5.89e+00	4.71e-02	1.23e-04	1.35e-08
2	0.3891251974368090e-02	6.94e+00	5.87e-01	3.45e-02	8.06e-05	8.24e-09
3	0.1914080223760730e-02	3.20e+00	1.62e-01	4.00e-02	1.08e-04	1.29e-09
4	0.1808123980030230e-02	9.93e-01	1.01e-01	8.70e-03	3.05e-05	3.28e-08
5	0.5935632599128700e-02	5.78e-02	6.59e-01	1.48e-02	3.48e-05	2.33e-08

(cf. (37)), and it demonstrates that the small-scale component of the surfaces translate precisely into significantly more diffuse scattering cross sections.

5. Conclusions

In conclusion, we have derived, implemented and exemplified the performance of a novel scheme for the numerical solution of scattering problems off surfaces that display multiple-scale characteristics. The procedure can be interpreted as providing a high-order version of the classical two-scale method [12, 14] in *both* the order of the perturbation and of the high-frequency asymptotic expansions. We have shown that this new approach can provide very accurate solutions in instances where the standard low-order versions fail and, thus, that it greatly expands on their domain of applicability. Moreover, we have further shown that the high-order nature of the approach allows for calculations in a regime that overlaps that where state-of-the-art direct solvers (e.g. based on integral equations [2]) are applicable and that, in this case, the current procedure can deliver quality solutions in a small fraction of the time necessary to produce similar results with these advanced algorithms. Extensions to shadowing and multiple scattering configurations, possibly based on ray-tracing and "localized integration" techniques [3] are left for future considerations.

Acknowledgments

Fernando Reitich gratefully acknowledges support from AFOSR through contract No. FA9550-05-1-0019, from NSF through grant No. DMS–0311763, and from the Army High Performance Computing Research Center (AHPCRC) under Army Research Laboratory cooperative agreement number DAAD19-01-2-0014.

Disclaimer. Effort sponsored by the Air Force Office of Scientific Research, Air Force Materials Command, USAF, under grant number FA9550-05-1-0019, and by AHPCRC under the auspices of the Department of the Army, Army Research Laboratory cooperative agreement number DAAD19-01-2-0014. The US Government is authorized to reproduce and distribute reprints for governmental purposes notwithstanding any copyright notation thereon. The views and conclusions contained herein are those of the author and should not be interpreted as necessarily representing the official policies or endorsements, either expressed or implied, of the Air Force Office of Scientific Research, the Army Research Laboratory or the US Government.

References

[1] Warnick K F and Chew W C 2001 Numerical simulation methods for rough surface scattering *Waves in Random Media* **11**, R1–R30

[2] Bruno O and Haslam M 2006 High-order solution of the scattering problem for one-dimensional perfectly-conducting periodic surfaces *Preprint*

[3] Bruno O, Geuzaine C, Monro A and Reitich F 2004 Prescribed error tolerances within fixed computational times for scattering problems of arbitrarily high frequencies: the convex case *Phil. Trans. Roy. Soc. London* **362**, 629-645

[4] Zhao Z, Li L, Smith J and Carin L 2005 Analysis of scattering from very large three-dimensional rough surfaces using MLFMM and ray-based analyses *IEEE Antennas and Propag. Mag.* **47** 20–30

[5] Liu P and Jin Y-Q 2004 The finite-element method with domain decomposition for electromagnetic bistatic scattering from the comprehensive model of a ship on and a target above a large-scale rough sea surface *IEEE Trans. Geosci. Remote Sens.* **42** 950–956

[6] Beckmann P and Spizzichino A 1963 *The Scattering of Electromagnetic Waves from Rough Surfaces: Part I. Theory* (London: Pergamon)

[7] Voronovich A G 1994 *Wave Scattering from Rough Surfaces* (New York: Springer-Verlag)

[8] Lynch P J 1970 Curvature corrections to rough-surface scattering at high frequencies *J. Acoust. Soc. Am.* **47** 804–815

[9] Liszka E G and McCoy J J 1982 Scattering at a rough boundary —Extensions of the Kirchhoff approximation *J. Acoust. Soc. Am.* **71** 1093–1100

[10] Chaloupka H and Meckelburg H 1985 Improved high-frequency current approximation for curved conducting surfaces *Arch. Elektron. bertragungstech.* **39** 245–250

[11] Rodriguez E 1989 Beyond the Kirchhoff approximation *Radio Sci.* **24** 681–693

[12] Kuryanov B F 1963 The scattering of sound at a rough surface with two types of irregularity *Sov. Phys. Acoust.* Engl. Transl. **8** 252–257

[13] Galybin N N 1976 Backscattering of sound by a distant sea surface *Soviet Physics-Acoustics* **22** 193–197

[14] McDaniel S T and Gorman A D 1983 An example of the composite-roughness scattering model *J. Acoust. Soc. Am.* **73** 1476–1486

[15] Lemaire D, Sobieski P, Craye C and Guissard A 2002 Two-scale models for rough surface scattering: Comparison between the boundary perturbation method and the integral equation method *Radio Sci.* **37** 1-1 – 1-16

[16] West J C and Ja S J 2002 Two-scale treatment of low-grazing-angle scattering from spilling breaker water waves *Radio Sci.* **37** 7/1 – 7/12

[17] Reitich F and Turc C 2005 High-order solutions of three-dimensional rough-surface scattering problems at high-frequencies. I: the scalar case *Waves in Random and Complex Media* **15** 1–16

[18] Reitich F and Turc C 2005 High-order solutions of three-dimensional rough-surface scattering problems at high-frequencies. II: the vector electromagnetic case *Waves in Random and Complex Media* **15** 323–337

[19] Bruno O, Sei A and Caponi M 2002 High-order high-frequency solutions of rough surface scattering problems *Radio Sci.* **37** 2/1-2/13

[20] Bleistein N and Handelsman R A 1986 *Asymptotic Expansions of Integrals* (New York: Dover)

[21] Bruno O, Sei A and Caponi M 2000 Rigorous multi-scale solver for rough-surface problems: High-order-high-frequency and variation of boundaries *Proceedings of NATO Sensors and Electronics Technology (SET) Symposium on "Low Grazing Angle Clutter: Its Characterization, Measurement, and Application"*

[22] Rice S O 1951 Reflection of electromagnetic waves from slightly rough surfaces *Comm. Pure Appl. Math.* **4** 351–378

[23] Valenzuela G R 1978 Theories for the interaction of electromagnetic and oceanic waves: A review

Boundary Layer Meteorol. **13** 61–85

[24] Bruno O P and Reitich F 1993 Numerical solution of diffraction problems: a method of variation of boundaries *Journal Opt. Soc. Am. A* **10** 1168–1175.

[25] Bruno O P and Reitich F 1993 Numerical solution of diffraction problems: a method of variation of boundaries II. Dielectric gratings, Padé approximants and singularities *Journal Opt. Soc. Am. A* **10** 2307–2316

[26] Bruno O P and Reitich F 1993 Numerical solution of diffraction problems: a method of variation of boundaries III. Doubly periodic gratings *Journal Opt. Soc. Am. A* **10** 2551–2562

[27] Lord Rayleigh 1945 *The theory of sound*, vol. 2, (New York: Dover) (1945)

[28] Wait J R 1970 Perturbation analysis for reflection from two-dimensional periodic sea waves *Radio Sci.* **6** 387–391.

[29] A. H. Nayfeh A H and O. R. Asfar O R 1974 Parallel–plate waveguide with sinusoidally perturbed boundaries *J. Appl. Phys.* **45** 4797–4800.

[30] E. Y. Harper E Y and F. M. Labianca F M 1975 Perturbation theory for scattering of sound from a point source by a moving rough surface in the presence of refraction *J. Acoust. Soc. Am.* **57** 1044–1051.

[31] E. Y. Harper E Y and F. M. Labianca F M 1975 Scattering of sound from a point source by a rough surface progressing over an isovelocity ocean *J. Acoust. Soc. Am.* **58** 349–364.

[32] Kuperman W A and Ingenito F 1977 Attenuation of the coherent component of sound propagating in shallow water with rough boundaries *J. Acoust. Soc. Am.* **61** 1178–1187.

[33] Anand G V and George M K 1986 Normal mode sound propagation in an ocean with sinusoidal surface waves *J. Acoust. Soc. Am.* **80** 238–243

[34] Anand G V and George M K 1993 Normal mode sound propagation in an ocean with random narrow–band surface waves *J. Acoust. Soc. Am.* **94** 279–292

[35] Lopez C, Yndurain F J and Garcia N 1978 Iterative series for calculating the scattering of waves from hard corrugated surfaces *Phys. Rev. B* **18** 970–972.

[36] Maradudin A A 1983 Iterative solutions for electromagnetic scattering by gratings *J. Opt. Soc. Am.* **73** 759–764.

[37] Monro A, 2007 Computation of a solution of scattering from a 2D periodic grating, PhD Thesis, Caltech.

[38] Nicholls D and Reitich F 2004 Shape deformations in rough surface scattering: cancellations, conditioning and convergence *J. Opt. Soc. Am. A* **21** 590-605.

[39] Nicholls D and Reitich F 2004 Shape deformations in rough surface scattering: improved algorithms*J. Opt. Soc. Am. A* **21**606-621.

[40] Jackson D R, Winebrenner D P and Ishimaru A 1988 Comparison of perturbation theories for rough–surface scattering *J. Acoust. Soc. Am.* **83** 961–969.

[41] Greffet J J 1988 Scattering of electromagnetic waves by rough dielectric surfaces *Phys. Rev. B* **37** 6436–6441.

[42] Wirgin A 1989 Scattering from hard and soft corrugated surfaces: Iterative corrections to the Kirchhoff approximation through the extinction theorem *J. Acoust. Soc. Am.* **85** 670–679.

[43] Greffet J J and Maassarani Z 1990 Scattering of electromagnetic waves by a grating: a numerical evaluation of the iterative–series solution *J. Opt. Soc. Am. A* **7** 1483–1493.

[44] Roginsky J 1991 Derivation of closed–form expressions for the T matrices of Rayleigh–Rice and extinction–theorem perturbation theories *J. Acoust. Soc. Am.* **90** 1130–1137.

[45] Greffet J J, Baylard C and Versaevel P 1992 Diffraction of electromagnetic waves by crossed gratings: a series solution *Opt. Lett.* **17** 1740–1742.

[46] Kazandjian L 1992 Comparison of the Rayleigh-Fourier and extinction theorem methods applied to scattering and transmission at a rough solid-solid interface *J. Acoust. Soc. Am.* **92** 1679–1691.

[47] Chesneaux J M and Wirgin A 1995 Response to comments on "Reflection from a corrugated surface revisited" *J. Acoust. Soc. Am.* **98** 1815–1816.

[48] V. I. Tatarskii 1995 Relation between the Rayleigh equation in diffraction theory and the equation based on Green's formula *J. Opt. Soc. Am. A* **12** 1254–1260.

[49] Bruno O P and Reitich F 1998 Boundary-variation solutions for bounded-obstacle scattering in three dimensions *J. Acoust. Soc. Am.* **104** 2579–2583.

[50] Bruno O P and Reitich F 2001 High-order boundary perturbation methods *Mathematical Modeling in Optical Science* Frontiers in Applied Mathematics Series (Philadelphia: SIAM) 71–109.

[51] Bruno O P and Reitich F 1992 Solution of a boundary value problem for Helmholtz equation via variation of the boundary into the complex domain *Proc. Roy. Soc. Edinburgh* **122A** 317–340.

[52] Chandler-Wilde S. N. and Zhang B 2003 Integral equation methods for scattering by infinite rough surfaces *Math. Meth. Appl. Sci.* **26** 463–488

[53] Dinesen P G and Hesthaven J S 2000 Fast and accurate modeling of waveguide grating couplers *J. Opt. Soc. Am. A* **17** 1565–1572

[54] Dinesen P G and Hesthaven J S 2001 Fast and accurate modeling of waveguide grating couplers. II. Three-dimensional vectorial case *J. Opt. Soc. Am. A* **18** 2876–2885

[55] Melrose R and Taylor M 1985 Near peak scattering and corrected Kirchhoff approximation for a convex obstacle, *Adv. in Math.* **55** 242–315

[56] Abramowitz M and Stegun I 1965 *Handbook of Mathematical Functions* (New York: Dover)

[57] Petit R. 1980 A tutorial introduction *Electromagnetic Theory of Gratings* (New York: Springer-Verlag) 1–40

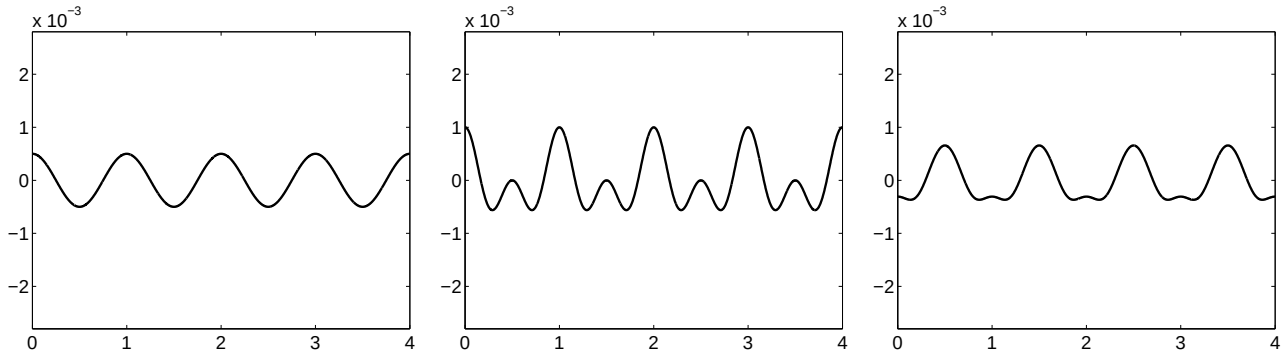

(a) $x_2 = S_0^{(1)}(x_1)$ (b) $x_2 = S_0^{(2)}(x_1)$ (c) $x_2 = S_0^{(3)}(x_1)$

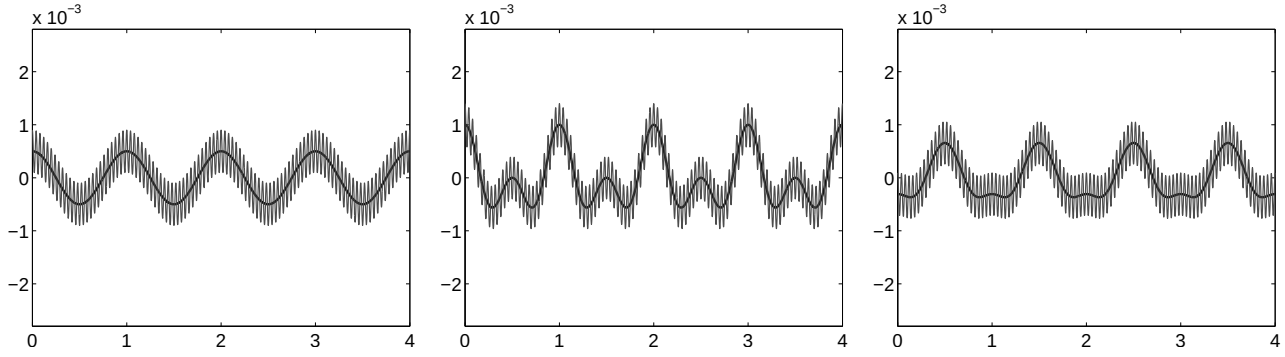

(d) $x_2 = S_1^{(1)}(x_1)$ (e) $x_2 = S_1^{(2)}(x_1)$ (f) $x_2 = S_1^{(3)}(x_1)$

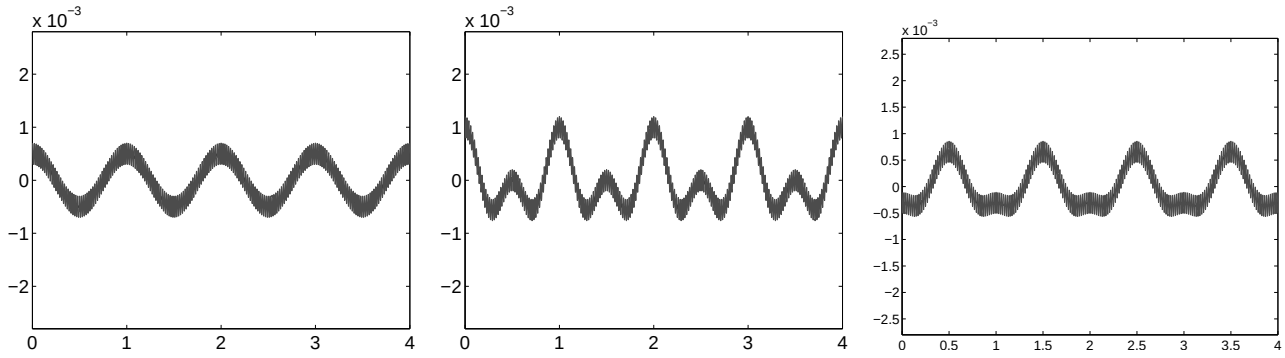

(g) $x_2 = S_2^{(1)}(x_1)$ (h) $x_2 = S_2^{(2)}(x_1)$ (i) $x_2 = S_2^{(3)}(x_1)$

Figure 1. Profiles for the examples of application of the multi-scale solver. Top: smooth component of the surfaces. Middle and Bottom: composite surfaces.

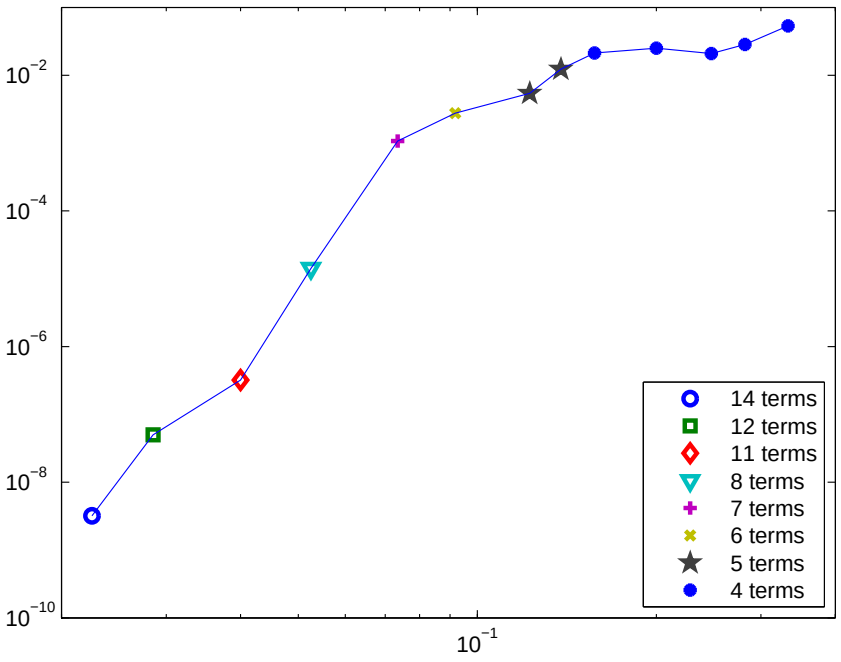

Figure 2. Logarithmic plots of the relative error in the backscattered energy $e_{0,0}$ vs. λ/R for the profile (36) and $i = 3$.

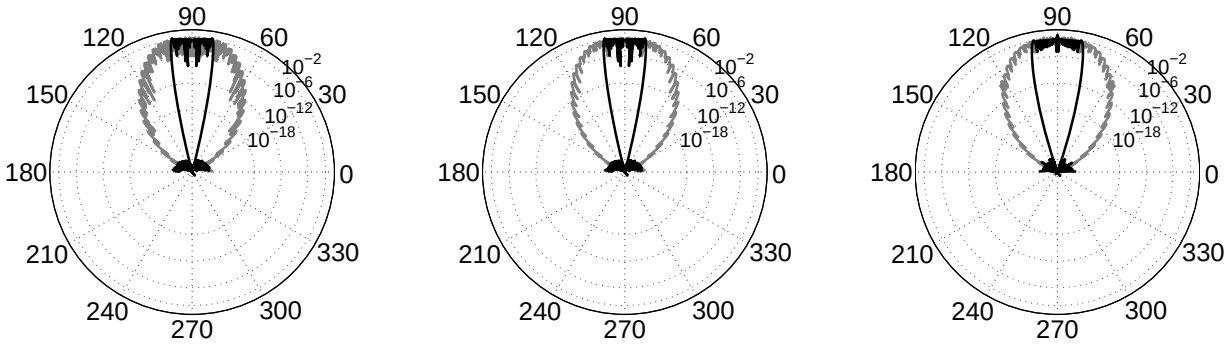

(a) $i = 1$ (b) $i = 2$ (c) $i = 3$

Figure 3. Polar plots of the efficiencies corresponding to the propagating modes: the inner contours correspond to the distributions of the scattered energy for the unperturbed profiles $S_0^{(i)}$, and the outer curves to that for the multi-scale profiles $S_0^{(i)} + F_1$ for the configurations in tables 18–20.